remote sensing

MDPI

Article

Simulation of the Impact of a Sensor's PSF on Mixed Pixel Decomposition: 1. Nonuniformity Effect

Chao Xu [1,2], Zhaoli Liu [1,*] and Guanglei Hou [1]

[1] Northeast Institute of Geography and Agroecology, Chinese Academy of Sciences, Changchun 130102, China; xuchao@iga.ac.cn (C.X.); houguanglei@iga.ac.cn (G.H.)

[2] College of Resources and Environment, University of Chinese Academy of Sciences, Beijing 100049, China

* Correspondence: liuzhaoli@iga.ac.cn; Tel.: +86-431-8554-2223

Academic Editors: Yudong Tian, Ken Harrison, Richard Müller and Prasad S. Thenkabail

Received: 29 January 2016; Accepted: 9 May 2016; Published: 21 May 2016

Abstract: The nonuniformity of the spatial response to surface radiation is a fundamental characteristic of all airborne and spaceborne sensors that inevitably introduces uncertainty into the estimation of object proportions by the spectral unmixing of mixed pixels. Simulated data of the surface radiation distribution and a TM (thematic mapper) response matrix were developed and utilized to imitate the generation of mixed pixels and the extraction of the object proportion via a Monte Carlo simulation, and then, the nonuniformity effect of a sensor's PSF (point spread function) was explored. The following conclusions were drawn: (1) given a nonuniform spatial response of a sensor to a surface scene with a constant object proportion and various object distribution patterns, the mixed pixel DN (digital number) of a remotely-sensed image becomes a random variable, which causes a PSF nonuniform effect on the object proportion extraction; (2) for the estimated object proportion, the corresponding true object proportion appears with a random variation; its upper and lower bounds take on an asymmetrical spindle shape; and models of these bound curves at any probability level were established; (3) there exists a negative linear relationship between the bias of the spectral unmixing and the estimated proportion; the bias is zero at an estimated proportion of 50%, and when the estimated proportions are approximately 100% and 0%, the object proportion is overestimated by 0.78% and underestimated by 0.78%, respectively; (4) the relationship between the standard deviation of the spectral unmixing and the estimated proportion follows a symmetrical polynomial function opening downward; the standard deviation reaches a maximum of 4.4% at the estimated proportion of 50%, and when the estimated proportion is approximately 100% or 0%, the standard deviation is a minimum, 1.05%. The above findings contribute to a comprehensive understanding of the PSF nonuniformity effect, have the potential to compensate for the bias of proportion estimation and present its confidence interval at any probability level.

Keywords: mixed pixel; spectral unmixing; sensor PSF; nonuniformity effect; Monte Carlo simulation

1. Introduction

Depending on the contrast between spatial resolution and object size, remote sensing includes two imaging modes, *i.e.*, low-resolution and high-resolution models [1]. In the former, a subpixel or linear subpixel occurs, which separately represents a small or linear object within the pixel, and in the latter, a boundary pixel usually exists, which is superimposed on the boundary between adjacent larger objects. All of them lead to a mixed pixel problem [2,3], which suggests that mixed pixels are ubiquitous in remote sensing images. More than one type of land cover occurs within mixed pixels, from which proportions of land covers are extracted by spectral unmixing. The approach has been widely applied to acquire information on natural resources, such as agriculture, forestry and minerals, and to monitor the ecological environment, including soil erosion, deforestation and forest fires [4].

The previous studies in this field can be mainly divided into two categories: models of spectral unmixing and the method of endmember selection, in which the model is further categorized as linear or nonlinear, and the method adopts different techniques depending on the presence of pure pixels [4,5]. Although great progress has been made in mixed pixel decomposition, most of the studies were conducted with the assumption that the spatial response of the sensor to the surface radiation, characterized as the spatial limitation and uniformity of the sensor response and described by a rectangular response function, was ideal [3,6]. However, in the actual imaging process, the spatial response takes the form of a point spread function (PSF), which is usually described by a two-dimensional normal distribution function [7,8]. Specifically, the intensity of the sensor response decreases away from the pixel center, which is referred to as the nonuniformity of the sensor's PSF [3,6]. In the meantime, the sensor not only responds to the surface radiation within a pixel, but also receives radiation energy from adjacent pixels, which is known as the adjacency of the sensor's PSF [2,9]. Both of them, which may be called the nonuniformity effect and adjacency effect, respectively, introduce significant uncertainty into the extraction of information from remote sensing images. In contrast with the impact upon the subpixel cover fraction inverted by spectral unmixing, the terminology of the spatial PSF nonuniformity effect was also applied to describe the radiometric inconsistencies among imaging spectrometry pixels caused by the distorted position and shape of the PSF in the spatial domain, which could be corrected through various interpolation methods [10], and there are essential differences between them.

The reconstruction of remotely-sensed images by a sensor's PSF has been used to improve the accuracy of mixed pixel decomposition, and the result showed that the estimation error in the areal proportion was reduced by up to 72% after the removal of the impact of the PSF [11]. Townshend *et al.* employed a simulated remote sensing image with an identical radiation of land cover type to explore the uncertainty in the proportion estimation under the adjacency effect of the sensor's PSF and found that the standard deviation of the estimation error decreased from 11% to 5.11% after the adjacency effect was eliminated using the designed deconvolution [9]. Subsequently, Huang *et al.* utilized four actual images representing different landscape types for further investigation, and the aforementioned conclusion was confirmed and extended [12]. However, their research merely discussed the adjacency effect of the PSF and did not touch upon the nonuniformity effect; in addition, the spatial responses of the sensor to the inside and outside of the pixel were all assumed to be uniform. Until now, there have been very few studies regarding the nonuniformity effect of a sensor's PSF on spectral unmixing. Using theoretical analysis and a simulation experiment, Manslow *et al.* analyzed the upper and lower boundaries of the true proportion variation of land cover against the estimated proportion extracted by spectral unmixing for the situation where the target objects were distributed over the central and marginal areas of the spatial extent of the sensor response, respectively [6]. The nonuniformity effect of the sensor's PSF on the spectral unmixing was better revealed; however, the study was restricted to only two extreme cases, and a comprehensive analysis of the nonuniformity effect for various spatial patterns of object distribution is lacking.

A mixed pixel in a remotely-sensed image may be understood to be the convolution of the nonuniform PSF of a sensor with the radiation distribution of a scene comprising different objects [3,13]. Without regard to the spectral variation of the land cover, the surface radiation distribution is only determined by the distribution pattern of ground objects, equivalent to the landscape pattern described by the sizes, shapes and spatial configurations of patches [14]. Manslow *et al.* conducted a theoretical analysis of the impact of PSF nonuniformity on spectral unmixing and assumed that a black circular target object was located in the center of a white square background, where both had identical areas and distinct reflections [6]. If the locations of the two objects were swapped, there was a significant difference in the DN (digital number) values of the mixed pixels generated by the nonuniform response of the sensor, and a variation in the estimated object proportion occurred. A subsequent simulation experiment also verified that theoretical analysis. Kaiser and Schneider constructed synthetic landscapes with simple object patterns to perform a spatial sub-pixel analysis, and a series of

spatial positions and rotation angles of objects was used [13]. The imaging processes were simulated on the basis of the PSF nonuniformity, and the resultant DNs of the mixed pixel varied with the above parameters, which better illustrated the role of the object distribution pattern. Calle *et al.* devised different patterns by altering the distance between a fire source and a mixed pixel center to investigate the influence induced by the PSF on detecting fire sources using images from the Meteosat Second Generation Spinning Enhanced Visible and Infrared Imager (MSG-SEVIRI) [15]. The results showed that the mixed-pixel DN changed and the estimated error of the brightness temperature rose when the distance increased, and for a distance of 3 km, the error was as large as 20 K. The above studies demonstrate that the nonuniform responses of sensors exert an influence on the extraction of remote sensing information through a change in the object distribution pattern. However, a very limited number of object patterns were taken into account, and the nonuniformity effect of the sensor's PSF could not be thoroughly revealed.

In this study, we explored the impact of the PSF nonuniformity of a sensor on object proportion extraction by spectral unmixing with an overall consideration of the object distribution pattern variation. The dataset representing various patterns was developed by the generation of raster images over a random object radiation distribution. The PSF parameters depicting the nonuniform response of the sensor were derived from measurement data related to Landsat-4 TM (thematic mapper), and a Monte Carlo method was employed to simulate the remote sensing imaging over the object distribution patterns and the object proportion extraction by linear spectral unmixing. We mainly focus on the following questions: (1) for a scene with certain object proportions and random distribution patterns, what impact does the PSF nonuniformity of the sensor have on the mixed-pixel DN? (2) For an estimated object proportion acquired by spectral unmixing, what is the statistical distribution of the corresponding true object proportions? (3) How do the bias and variance of the object proportion estimation change with the estimated proportion?

2. Mechanism Analysis

For a clear explanation of the nonuniformity effect, the adjacency effect of the sensor's PSF is neglected here. In this case, the response range of the sensor's detectors equals the pixel size, namely the ground instantaneous field of view (GIFOV). The scene radiation distribution is composed of a two-dimensional array of infinitesimal point light sources; the radiation at spatial location (u, v) is represented by $R_t(u, v)$; and t denotes the object type. Correspondingly, the spatial response of the sensor's detector is represented as a two-dimensional array of infinitesimal impulses, whose central position (x, y) is the pixel center, and the response capability of each impulse is represented by its spatial response function (SRF), *i.e.*, SRF (u−x, v−y), which is the sensitivity of the sensor's detector to the point light source at the location (u−x, v−y).

The radiation signal recorded by the mixed pixel can be described as a convolution of the scene radiation distribution with the spatial response function of the sensor; however, it must undergo signal amplification and AD conversion, and the resultant DN of the mixed pixel is expressed as:

$$DN_{mix}(x, y) = D\left[R_t(u, v) * SRF(u - x, v - y)\right] \quad (1)$$

where D[.] denotes the quantization of the radiation signal acquired by a detector unit and * refers to the convolution operation.

If the continuous spatial response function and the scene radiation distribution field are separately discretized into regular square two-dimensional cell arrays and the center of an image pixel is regarded as the origin of the coordinate system, the mixed-pixel DN may be rewritten as:

$$DN_{mix} = D\left[\sum_{i=-n}^{n}\sum_{j=-n}^{n} R_t(i\Delta, j\Delta) \times SRF(i\Delta, j\Delta)\right] \quad (2)$$

where Δ is the cell size, n is a positive integer, (2n + 1) is the row or column number of the square arrays and $(i\Delta, j\Delta)$ is the spatial location of any cell in the arrays for $u = i\Delta$ and $v = j\Delta$.

When the spatial response of a sensor's detector to the scene radiation array is uniform, it can be described by a discrete two-dimensional rectangular distribution function:

$$\mathrm{Rect}(i\Delta, j\Delta) = \begin{cases} \frac{1}{(2n+1)^2} & , |i| \leqslant n \text{ and } |j| \leqslant n \\ 0 & , \text{otherwise} \end{cases} \tag{3}$$

If the surface scene array imaged by the sensor's detector comprises target and background object cells, their distribution patterns can randomly change and, in addition, their cell radiation values separately hold the fixed values of R_o and R_b, the DN value of the mixed pixel can be represented as:

$$\begin{aligned} DN_{mix} &= D\left[N_o R_o \mathrm{Rect}\left(i\Delta, j\Delta\right) + N_b R_b \mathrm{Rect}\left(i\Delta, j\Delta\right)\right] \\ &= D\left[\tfrac{N_o}{N_t} N_t R_o \mathrm{Rect}\left(i\Delta, j\Delta\right) + \tfrac{N_b}{N_t} N_t R_o \mathrm{Rect}\left(i\Delta, j\Delta\right)\right] \\ &= P_o D\left[N_t R_o \mathrm{Rect}\left(i\Delta, j\Delta\right)\right] + P_b D\left[N_t R_b \mathrm{Rect}\left(i\Delta, j\Delta\right)\right] \\ &= P_o DN_o + P_b DN_b \end{aligned} \tag{4}$$

where N_o and N_b are the numbers of target and background object cells, respectively, their total, the proportions of the two types of objects are $P_o = N_o/N_t$ and $P_b = N_b/N_t$ and DN_o and DN_b are the DN values of their pure pixels.

Equation (4) is the fundamental expression of the popular linear spectral unmixing technique, and the target object proportion is derived from:

$$P_o = \frac{DN_{mix} - DN_b}{DN_o - DN_b} \tag{5}$$

In reality, a remote sensor responds to the scene radiation field through a nonuniform PSF; the two-dimensional normal function is typically employed to depict its spatial response. If the spatial sensitivities in the x- and y-coordinate directions are mutually independent, their standard deviations (σ) are equivalent, and the center of the mixed pixel is the origin of the coordinate system; the discrete mathematical expression of the sensor's PSF is:

$$\mathrm{PSF}(i\Delta, j\Delta) = \frac{1}{2\pi\sigma^2} e^{-\left[\frac{(i\Delta)^2 + (j\Delta)^2}{2\sigma^2}\right]} \tag{6}$$

It can be observed from Equation (6) that the sensor sensitivity varies with the shift of the spatial location $(i\Delta, j\Delta)$ within a mixed pixel. The spatial response function is convolved with the scene radiation array, and the resultant DN value of the mixed pixel can be rewritten as:

$$DN_{mix} = D\left[\sum_{k=1}^{N_o} R_o \mathrm{PSF}(i\Delta, j\Delta) + \sum_{k=1}^{N_b} R_b \mathrm{PSF}(i\Delta, j\Delta)\right] \tag{7}$$

Equation (7) is obviously distinct from Equation (4) because the sensor's detector responds differently to the same scene cell radiation at different locations. Therefore, the cells of the same object type cannot be grouped as in Equation (4). This phenomenon can be elucidated by Figure 1a,b; they have the same object distribution patterns as Figure 1c,d, respectively, and their target object proportions have the same value of 5/16. Under the nonuniform response of the sensor, two different object distribution patterns lead to two distinct mixed pixel DNs (DN2 and DN3). This means that the mixed-pixel DN relative to a certain object proportion is a random variable and that the application of the linear spectral unmixing model (Equation (5)) to an actual remote sensing image inevitably causes an uncertainty in the object proportion extraction.

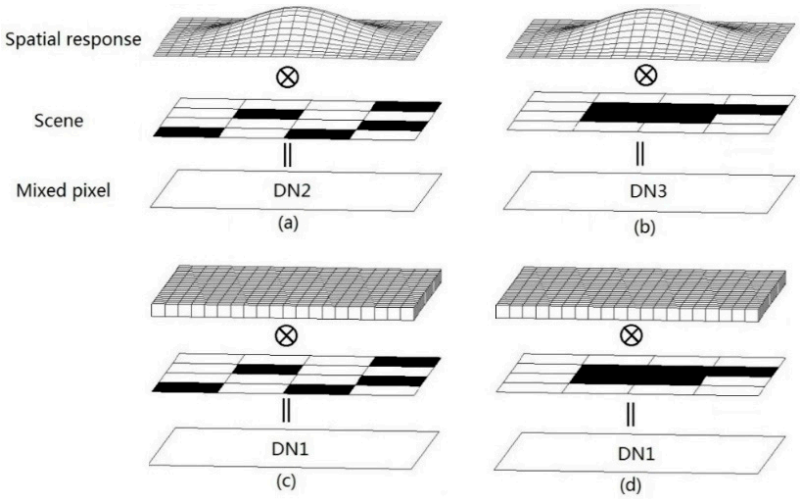

Figure 1. Schematic diagram of the impact of the nonuniform spatial response of the sensor's detector on the DN value of a mixed pixel. (**a**) and (**b**) represent the imaging processes of surface scenes with different object distribution patterns and an identical areal proportion of 5/16 (the black and white cells indicate the target and background objects, respectively). The DN value of the mixed pixel in (**a**) (DN2) is distinguished from the one in (**b**) (DN3) by the nonuniform spatial response of the sensor's detector with a two-dimensional normal function. The scenes in (**c**) and (**d**) are the same as those in (**a**) and (**b**), respectively, but in the case of a uniform two-dimensional rectangle function of a sensor's spatial response, the mixed pixels generated by the convolution operation have the same DN value (DN1).

The spectral unmixing has nothing to do with the object distribution pattern in the mixed pixel when the spatial response of the sensor is assumed to follow a uniform rectangle distribution function. Figure 1a,c more visually illustrate this deduction through the imaging processes of two scenes with identical object proportions and different distribution patterns. The proportions of the target object (black cell) in the two scenes are all 5/16, but the target object cells are dispersed in Figure 1a,b; in other words, their object distribution patterns are different, and then, their mixed pixel DNs take the same value of DN1. Therefore, no matter how the object distribution pattern changes, the object proportion obtained by spectral unmixing is uniquely determined under the uniform spatial response of the sensor.

In the real world, a surface scene can be approximated by two-dimensional lattice data with a fairly small cell size. In that way, there are a considerable number of object distribution patterns for a given object proportion, and the number of mixed pixels that can be produced by the nonuniform response of a sensor is also immense. Conversely, for the determined DN of a mixed pixel, the object proportion estimated by the spectral unmixing is a unique value, but the number of its corresponding true object proportions is enormous for a vast array of object distribution patterns. Consequently, the impact of the PSF nonuniformity on the spectral unmixing is reflected in the statistical distribution of the true object proportion varying around the estimated one and is delineated by the relationship between the estimated object proportion and the statistical parameters of the proportion estimation error; the latter variable includes the bias and variance of the proportion estimation error.

3. Method

Due to the complicated process of remote sensing and the difficulty of an overall quantification of the object distribution pattern, it is impossible to establish a perfect uncertainty model of spectral unmixing by mathematical analysis [6]. Monte Carlo simulation was employed here to investigate the impact of PSF nonuniformity on spectral unmixing and was executed using the MATLAB software platform because of its powerful capabilities; the specific steps are as follows.

3.1. Simulated Data of the Scene Radiation Distribution

A two-dimensional matrix was employed to represent the scene radiation distribution. Considering the quantization level of the actual image, the symmetry of the spatial response function and the computational complexity of the simulation, the size of the scene radiation matrix was defined as 17 × 17, and the total number of matrix elements was $N_t = 289$. The matrix consisted of target and background object elements, and the radiation values of their elements were set to 289 and 0, respectively, namely $R_o = 289$ and $R_b = 0$. The series data of the true target object proportion (P_o) were acquired by incrementally increasing the target element number (N_o), such that $P_o = N_o/N_t$. The true target proportion ranged from 0 to 100%, with an increment of 1/289, and the number of the true target or background proportion was 290.

The scene radiation matrices that reflected the random variation of the object distribution pattern were produced by the following procedure. First, for a true proportion of the target object, a certain number of target elements was randomly drawn from the 17 × 17 matrix, and the others were regarded as background elements. Second, the elements of the target and background objects were assigned their predetermined radiation values. Third, the above operation was repeated, and the new matrix for another distribution pattern was in turn compared to each of the previous ones. If the two of them were exactly the same, the new matrix was discarded. Fourth, the number of generated matrices was accumulated, and if the total number reached ten thousand, the generation of matrices for the given proportion ended. Finally, according to the above steps, the simulated data of the scene radiation distributions for each object proportion was successively established.

3.2. Spatial Response Matrix of the Sensor's Detector

Although there have been many studies of the parameters of the TM sensor's PSF, most of those studies have not reported its variance parameter [7,8,16]. Based on an inquiry into several relevant reports, it was found that McGillem *et al.* obtained raw data of high quality with respect to the PSF of Landsat-4 TM in the across-track direction [7], and its variance parameter could be derived from their paper. The specific derivation process was as follows. To begin, using computer graphics software, the image copied from Figure 1 was magnified, and the x coordinates of the data points and their grey values were exactly determined and read out. Next, the original data were fitted by a Boltzmann function; moreover, the model curve was differentiated to obtain the derivative data relative to the x coordinates of the data points and, therefore, to acquire the experimental data of the TM sensor's PSF. Once again, in the x coordinate direction, the experimental data were standardized, namely the population mean was subtracted from the x values of the data points, and the differences were divided by their population variance to compare the PSF nonuniformities of different types of sensors. In the y coordinate direction, the experimental data were normalized; specifically, the y values of the data points were divided by their sum to eliminate the effect of variations in the surface radiation in the experimental data, which was different from the normalization using the y maximum in previous research. Finally, the treated experimental data were fitted using a one-dimensional normal function to obtain the variance parameter of the TM sensor's PSF, and the resultant standard deviation σ was equal to 0.9197.

It was necessary to rasterize the sensor's spatial response and to limit its spatial extent for the spatial match between the scene radiation distribution and the spatial response function. The theoretical extension of the sensor's PSF as represented by a two-dimensional normal function is boundless, but 99.7% of the total surface radiation is contained within a region 3σ from the pixel center; the PSF spatial extent was specified to [−3σ, 3σ], and the spatial extent of the TM PSF was separately established as [−2.7591, 2.7591] in the track and scan directions. The PSF was discretized into a regular grid of 17 × 17, and each cell of the grid was assigned the value of a standard normal function at the cell center; thereby, the spatial response matrix of the TM sensor was acquired. In addition, the matrix was once more normalized, as the exterior part of the PSF was discarded and the interior part discretized.

3.3. Simulation of Mixed Pixel Generation and Its Spectral Unmixing

The mixed pixel was generated using a convolution operation, specifically the summation of each element in the scene radiation matrix weighted by the spatial response matrix. The output DNs of the pure pixels of the target and background objects were assigned a maximum of 289 and a minimum of 0, whereas the output DNs of the mixed pixel ranged from 0 to 289. Through rounding, the resultant pixel DNs had 290 quantization levels.

Under a given proportion of target objects, the object distribution pattern within a mixed pixel is unknown, and the probability of each pattern occurrence is $1/C_{N_t}^{N_o}$, following a uniform distribution function. Ten thousand scene radiation matrices for each true object proportion were used as object distribution pattern samples, and ten thousand mixed pixel DNs were generated. However, when the object proportion is approximately 0% or 100%, *i.e.*, when the number of target cells becomes close to 0 or 289, the number of object distribution patterns for each target object proportion $C_{N_t}^{N_o} = C_{289}^{N_o}$ is less than ten thousand, and the number of mixed-pixel DNs is also below ten thousand.

The pure pixel DN_o and DN_b of the target and background objects were equivalent to their radiation values R_o and R_b, respectively, *i.e.*, $DN_o = 289$ and $DN_b = 0$, and then, the equation for the linear spectral unmixing (Equation (5)) was simplified as $P_o = DN_{mix}/289$, which reflects the one-to-one relationship between the mixed-pixel DN and estimated target proportion and which was utilized to acquire the estimated target proportion.

4. Results

4.1. Impact of PSF Nonuniformity on the Mixed-Pixel DN

For each true object proportion, the mixed pixels with the same DN were counted, and the summation array was divided by the total number of mixed pixels to produce the frequency distribution of the mixed-pixel DNs. In an ascending sequence of the true object proportion, the frequency distributions, represented as column data, were combined into a frequency matrix of 290×290. Figure 2 presents the frequency distribution of the mixed-pixel DNs *versus* the true object proportion.

For the true object proportions of 5% and 50%, the frequency distributions of the-mixed pixel DNs are shown in Figure 2a,b, respectively. For an object proportion of 50%, if the sensor spatial response is represented by a rectangular distribution function, the mixed-pixel DN has a unique value of 145; if the sensor is represented by the normal distribution function, the mixed-pixel DN becomes a random variable varying around the DN value of 145. The DNs seemingly follow a one-dimensional normal distribution, and most of them fall within the range of 95 to 195, with a maximum frequency of approximately three. For the object proportion of 5%, the mixed pixel DNs were distributed roughly in the interval between five and 45, and their frequency distribution was reduced by more than half and became an asymmetric pattern with an increasing maximum frequency of approximately six.

Under the nonuniform spatial response of the sensor's PSF, the frequency distribution of the mixed-pixel DNs against the true object proportion takes the shape of a spindle, with a wider middle and narrow ends (Figure 2). As the true proportion approaches 50%, the frequency distribution tends to flatten, whereas it becomes very sharp as the true proportion approaches 0% or 100%. In contrast, when the spatial response of the sensor follows a rectangular distribution function, only a single DN of the mixed pixel is generated, and its change with the true object proportion is expressed by the black bold line in Figure 2, which indicates that there was a one-to-one relationship between the true object proportion and the mixed-pixel DN. According to the formula of the linear spectral unmixing, $P_o = DN_{mix}/289$, it is inferred that for the nonuniformity of the sensor's PSF, the estimated object proportion has the same statistical characteristics as the mixed-pixel DN through the random variation of the object distribution pattern.

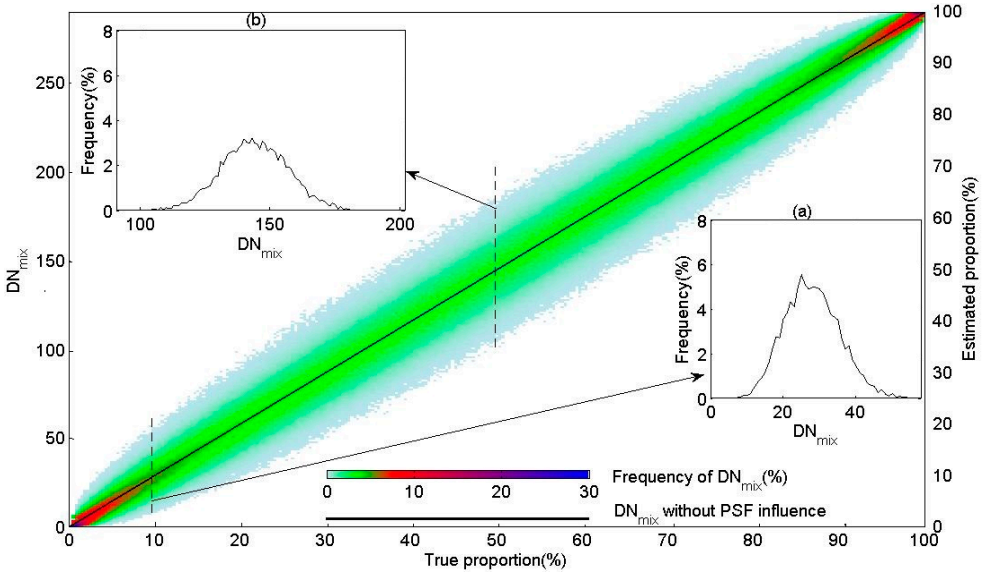

Figure 2. Frequency distribution of the mixed-pixel DN (DN_{mix}) and the estimated *versus* true proportion of the target object given the nonuniformity of the sensor's PSF. (**a**) and (**b**) show the frequency distributions of the DN_{mix} for true proportions of 6% and 50%, respectively. The thick black bold line indicates the relationship between the true proportion and DN_{mix} and the estimated proportion for the uniform rectangular response function of the sensor.

4.2. Impact of the PSF Nonuniformity on the Spectral Unmixing

4.2.1. Probabilistic Description of the Uncertainty in the Spectral Unmixing

The above analyses reveal only the cause of the spectral unmixing uncertainty under the impact of PSF nonuniformity. However, in an actual decomposition of mixed pixels, only the estimated object proportion is obtained. To analyze the specific influence of the PSF nonuniformity, the left and right coordinate axes in Figure 2 were swapped, and the frequency distribution matrix was entirely inverted along the black solid line. A frequency distribution matrix of the true object proportion *versus* the estimated object proportion was generated, which suggests that there is a one-to-many relationship between them, *i.e.*, one estimated proportion corresponds to various true proportions.

The diagonal element of the frequency matrix against a given estimated proportion was taken as the center of the column array, and the half-frequency of the central element was added to that of the adjacent element on one side. If the accumulation was below 25% of the column frequency summation, another adjacent element was sequentially incorporated to accumulate the unilateral frequency until the cumulative value exceeded 25%. The two final elements in the column array were used as the upper and lower bounds of the confidence interval of the estimated proportion at the 50% confidence level. The above procedure was repeated, and the bounds for all of the estimated proportions were acquired. The upper and lower bounds at the 90% confidence level were obtained in the same way. In addition, the two extremes of the scene radiation matrix, all cells of the target object over its boundary or center, were separately convolved with the spatial response matrix. From the resultant mixed-pixel DNs, the maximum and minimum of the true object proportion for each estimated proportion were derived, and the upper and lower bounds at the 100% confidence level were determined. Figure 3 shows the upper and lower bounds of the confidence interval of the estimated proportion at the 50%, 90% and 100% probabilities.

The subfigure in Figure 3 shows the frequency distribution of the true proportion at an estimated proportion of 50%. The central dashed line indicates the true proportion of 50%, around which the true proportion randomly varies, and it is mainly distributed in the range between 40% and 60%, with a probability of occurrence of approximately 90%. It can be observed from Figure 3 that these upper

and lower bounds at a confidence level of less than 90% take a fusiform shape similar to that of the frequency distribution of the mixed-pixel DN, whereas at a confidence level of 100%, the fusiform shape takes an asymmetrical form and rapidly swells. More specifically, on the one hand, at the 90% confidence level, the frequency distribution of the true proportion is relatively concentrated, and the confidence interval is slightly larger than that at the 50% confidence level, whereas it sharply increases more than five times at the 100% confidence level; conversely, the confidence interval attains a maximum width when the estimated proportion is 50%, and it gradually becomes narrower and tapers out when the estimated proportion tends to 0% or 100%.

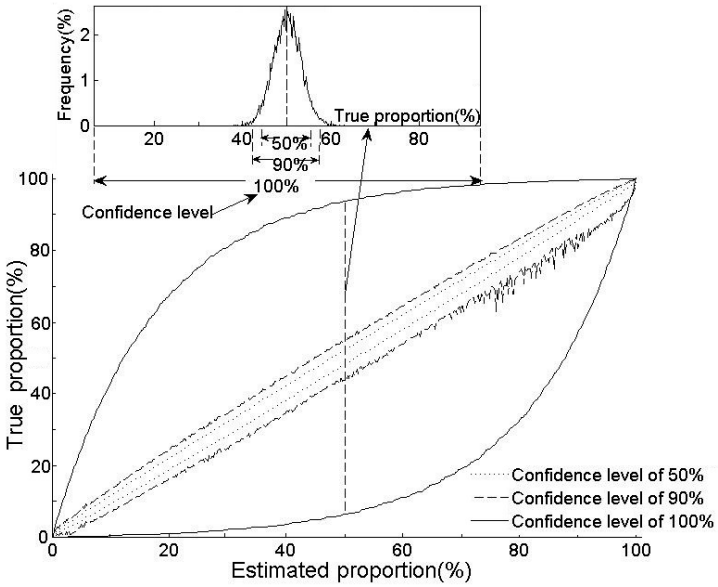

Figure 3. Upper and lower bounds of the confidence interval of the true object proportion *versus* its estimated proportion at three different confidence levels. The subfigure shows the frequency distribution of the true object proportion at an estimated proportion of 50%.

To further depict the frequency distribution of the true proportion, representing the uncertainty of the spectral unmixing, the model proposed by Manslow and Nixon [6] was modified and applied to fit the data series of the upper and lower boundaries at different confidence levels; the formulas are expressed as follows.

For the lower boundary curve of the confidence interval,

$$y_{min} = 1 - \frac{1}{2t\alpha^4}\ln|e^{(2t\alpha^4)} - e^{(2t\alpha^4 p_1)} + 1| \tag{8}$$

and for the upper boundary curve of the confidence interval,

$$y_{max} = \frac{1}{2t\alpha^4}\ln|e^{(2t\alpha^4)} - e^{[2t\alpha^4(1-p_2)]} + 1| \tag{9}$$

where α is the variance parameter of the TM sensor's PSF, specified as 0.9197, p1 and p2 are given by the two following expressions and x is the estimated proportion.

$$\begin{aligned} p_1 &= 0.3x\frac{e^x-1}{e-1} + (1-0.3x)\frac{\ln(x+1)}{\ln 2} \\ p_2 &= 0.7(1-x)\frac{e^x-1}{e-1} + (0.7x+0.3)\frac{\ln(x+1)}{\ln 2} \end{aligned} \tag{10}$$

In addition, t is a variable related to the confidence level that was obtained through the fitting of the bound data of many confidence levels; the results are shown in Table 1.

Table 1. Fitting data of parameter t in the bound model of the confidence interval.

Confidence Levels (c)	0%	30%	50%	70%	90%	100%
t	0.01	0.15	0.24	0.32	0.5	2.00

A model of the relationship between the parameter t of the bound model and the confidence level c was established and can be used to predict t at any confidence level:

$$t = \exp(6.533c^2 - 0.6835c - 5.164) - 0.0057(r^2 = 0.9713) \quad (11)$$

By constructing a series of mathematical models, the variation range of the corresponding true proportion at any confidence level can be accurately forecasted for each estimated proportion; therefore, the uncertainty in the spectral unmixing caused by the nonuniformity of the TM sensor's PSF can be comprehensively described.

4.2.2. Systematic Error of the Spectral Unmixing

In the above section, only the frequency distribution of the true proportion was described for the impact of the PSF nonuniformity, and a thorough analysis of the statistical characteristics of the proportion estimation error has not yet been conducted. Therefore, the various true proportions in relation to each estimated proportion were averaged, and then, the average was subtracted from the estimated proportion. Their difference was used to characterize the systematic error of the object proportion extraction under the influence of the PSF nonuniformity, which is referred to as the bias of the spectral unmixing.

Figure 4a displays the change pattern of the bias of the spectral unmixing with the estimated proportion. It can be determined that there is a close negative linear relationship between the estimated object proportion and the bias of the proportion estimation. With the increase in the estimated proportion from 0% to 100%, the estimation bias decreases from 0.78% to −0.78%, and it equals 0% at an estimated proportion of 50%, which demonstrates that in the extraction of the object proportion by spectral unmixing, if the estimated proportion is below 50%, it must be larger than the mean of the true proportions, *i.e.*, the spectral unmixing overestimates the object proportion. However, when the estimated proportion is greater than 50%, it is less than the mean of the true proportions, *i.e.*, the spectral unmixing underestimates the object proportion. The absolute value of the bias approaches the maximum value when the estimated proportion is approximately 0% or 100%, but it is much smaller, not exceeding 1%.

The relationship between the estimated proportion and its estimation bias was fitted with a linear model to predict the deviation of the estimated proportion from the averaged true proportion,

$$B_e = -0.0156P_e + 0.78(r^2 = 0.984) \quad (12)$$

where B_e is the estimation bias, and p_e is the estimated proportion, with a defined domain of (0%, 100%).

The systematic error of the object proportion extraction indicates that the frequency distribution of the true proportion relative to the estimated one is asymmetrical, which can be quantitatively represented by a skewness coefficient. Figure 4b shows that the skewness of the true proportion distribution was positive when the estimated proportion was less than 50%, implying that the tail extends more towards a large value and its peak deflects towards a small value; when the estimated proportion exceeded 50%, the frequency distribution behaved conversely, which basically coincides with the change in the spectral unmixing bias. In addition, the skewness coefficient changed more gently when the estimated proportion ranged from 10% to 90%, and beyond that range, the skewness coefficient varied sharply.

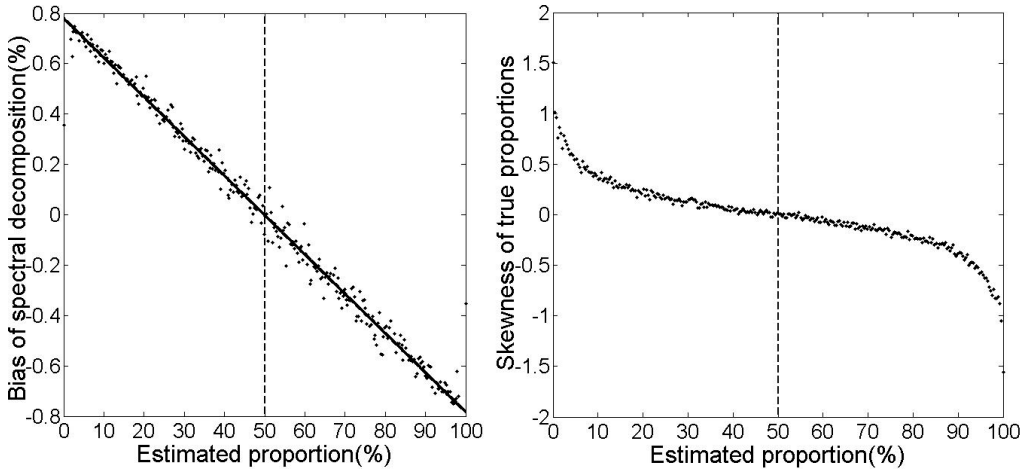

Figure 4. Bias of the spectral unmixing and skewness of the true proportion distribution *versus* the estimated proportion. The solid line in (**a**) is the linear fitting curve of the bias, and the dashed lines in (**a**) and (**b**) indicate an estimated proportion of 50%.

4.2.3. Random Error of the Spectral Unmixing

The true proportion in relation to an estimated proportion is a random variable, which implies that the estimation error of the object proportion is also a random variable, and its standard deviation can be used to portray the dispersion of the proportion estimation (*i.e.*, the random error) well. The statistical parameter for each estimated proportion was calculated one at a time, and the random error of the object proportion extraction, or the standard deviation of the spectral unmixing, which is also caused by the nonuniformity of the sensor's PSF, is shown in Figure 5a.

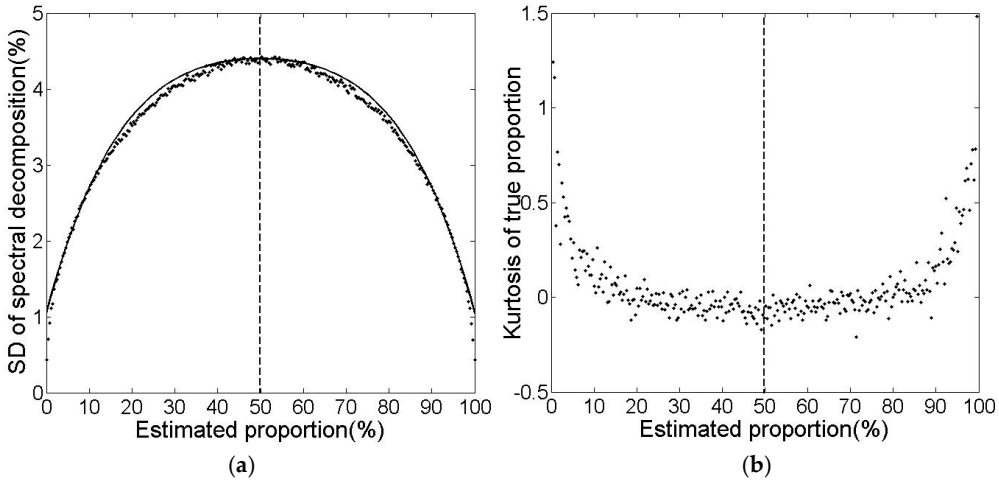

Figure 5. Standard deviation of the spectral unmixing and kurtosis of the true proportion distribution *versus* the estimated proportion. The solid line in (**a**) is the fitting curve of the standard deviation, and the dashed lines in (**a**) and (**b**) indicate the estimated proportion of 50%.

It can be seen that the standard deviation of the true proportion as a function of the estimated proportion can be depicted with a polynomial equation with an asymmetrical shape opening downward. The curve apex at an estimated proportion of 50% suggests a standard deviation maximum of approximately 4.4. With the extension of the estimated proportion towards 0% and 100%, the standard deviation shows an accelerated downward trend and finally reaches a minimum. Because

the maximum of the standard deviation is approximately five-times higher than that of the bias, the random error of the spectral unmixing should not be ignored in the extraction of the object proportion.

A polynomial function was chosen to portray the change in the standard deviation of the true proportion as a function of the estimated proportion:

$$SD_e = -3.11 \times 10^{-7}(P_e - 50)^4 - 5.64 \times 10^{-4}(P_e - 50)^2 + 4.4 \, (r^2 = 0.968) \quad (13)$$

where SD_e is the standard deviation and Pe is the estimated proportion, with the defined domain of (0%, 100%). The model can be applied to predict the standard deviation of the spectral unmixing from the PSF nonuniformity.

Figure 5b displays the kurtosis coefficient of the frequency distribution of the true proportion, which can reflect the degree of sharpness of the top of the distribution curve. The change in the kurtosis with the estimated proportion shows a symmetric pattern; the coefficient takes a minimum value at an estimated proportion of 50%, and with the increase or decrease of the estimated proportion, it rises slowly until 20% or 80% of the estimated proportion, after which it sharply increases and surpasses one. The change trend of the kurtosis coefficient may better correspond to that of the standard deviation of the spectral unmixing; for instance, when the estimated proportion was approximately 0% or 100%, the kurtosis coefficient approached the maximum, whereas the standard deviation approached the minimum.

5. Discussion

The nonuniformity of the spatial response of a sensor to the surface radiation introduces uncertainty into spectral unmixing, the reason for which was profoundly explored through the theoretical analysis and simulation experiment described in this paper. The results of the research show that the nonuniformity of a sensor's PSF exerts an influence on the object proportion extraction only through a change of the object distribution pattern. Calle *et al.* also noted that the shape of the MTF(modulation transfer function) (*i.e.*, the PSF nonuniformity) did not affect the measurement of the fire temperature for a uniform distribution of surface radiation [15], which means that the PSF nonuniformity had no effect on a homogeneous surface without an object distribution pattern. A spatial subpixel analysis was used to obtain information of a simple object distribution pattern within mixed pixels [13], from which the object proportion could also be derived. Due to the ubiquity of complex object distribution patterns and the impact of PSF nonuniformity, the method cannot obtain exact object proportion information. Although exact data on the object distribution patterns can be provided, it is impossible to comprehensively describe those patterns with one or a few quantitative indicators; the number of landscape metrics for the description of a spatial pattern in landscape ecology may be almost one hundred [14]. Therefore, to determine an object proportion using spectral unmixing, the object distribution pattern inevitably must be treated as a random variable.

In theory, the spatial distribution pattern arises from the spatial autocorrelation of the Earth's surface properties being measured by spatial statistics, such as Moran's I and Geary's C, and ranging from a uniform pattern through a random pattern to a clustered pattern [17]. The simulated data of the scene radiation distribution in this study corresponds to the entire spatial pattern continuum. However, a specific area could only occupy a span of the spatial pattern continuum; in other words, the object spatial distribution takes on a certain landscape pattern in the form of the size, shape and configuration of patches [14], and the diverse object distributions across the entire spatial pattern continuum generally do not occur. Actually, the spatial pattern at the subpixel scale is usually unknown before spectral unmixing is carried out, so any object distribution pattern may emerge with the same probability of occurrence; in addition, the random nature of the image pixel position relative to a ground cover also accumulates the randomness of the object spatial distribution. Various pattern changes are embodied in the simulated scene radiation distribution dataset, and it is reasonable to employ such data to study the PSF nonuniformity effect.

The simulation data comprehensively represents the random variation of an object distribution pattern, and relevant parameters, such as the object proportion, were also precisely controlled, so the PSF nonuniformity effect was sufficiently revealed. In previous research on the impact of a sensor's PSF, simulated or real remote sensing images were employed [9,12]. These images may have contained some types of object distribution patterns, but the full diversity of those patterns was not considered. In addition, only an average of the proportion estimation errors was provided, and estimation errors with regard to different estimated proportions were lacking. Manslow and Nixon employed raster data simulating object distribution patterns, but they represented only two types of extreme cases, such that target objects were separately located on the fringe and in the central zones, even though the upper and lower bounds of the true proportion variation *versus* the estimated proportion were given [6].

Pont *et al.* explored the influence of a sensor's PSF on the statistics of a multispectral target signature; the mean and covariance of the target signature were described [18]. Park and Schowengerdt conducted a study on the impact of a sensor's PSF on the scan imaging of an object's edge, which was characterized by both the system and random errors [19]. In the research on the impact of a sensor's PSF on object proportion extraction, the mean error of the proportion estimation has been well discussed [9,12], but those works lacked an analysis of the variance of the object proportion estimation. The uncertainty model established in this paper includes both system and random errors of the object proportion estimation, which present a comprehensive description of the effect of PSF nonuniformity on the decomposition of mixed pixels. Manslow *et al.* made a thorough inquiry of the maximum range of the true proportion variation in relation to any estimated proportion using simulated data with two extreme object distribution patterns [6]. Our study is somewhat similar to theirs in the shape of the upper and lower bounds of the true proportion variation; however, the fusiform shape of the former appears to be wider than the latter. The reason lies in the difference in the ways by which they acquired the bounding curves. For the generation of the lower bound, their procedure included an additional step that a target object located in the fringe zone was redistributed to the central zone. Because of the maximum response in the center of the PSF, the enlarged mixed-pixel DN certainly increased the lower bound of the true proportion variation; in the same way, the upper bound was reduced. Moreover, the models describing the bound curves were expanded here and can represent the bounds of the true proportion variation at any probability level. In addition to the nonuniformity of the sensor's PSF, the intra-class spectral variability may also bring about the distribution of the object proportion estimations (*i.e.*, possible class compositions) [20], and the error of the subpixel cover fraction inverted by spectral mixture analysis might be mitigated through different techniques of endmember variability reduction [21].

The simulated raster data with cells of fixed size were acquired using a random sampling with a limited sample size and cannot perfectly represent the true variation of the surface radiation distribution; therefore, there must be some flaws in the research results. For example, when the estimated proportion was approximately 0% or 100%, the predicted standard deviation of the proportion estimation was 1.05% using the random error model, whereas its theoretical value is 0%. Even so, the uncertainty model of spectral unmixing can still better describe the impact of the PSF nonuniformity on object proportion extraction. The aforementioned uncertainty models of spectral unmixing (Equations (12) and (13)) may be utilized to represent the mode of the PSF nonuniformity effect for a certain type of sensor, and the models have a better generality if the relevant parameters of the sensor's PSF are considered. The assumption that the PSF spatial extent is equal to pixel size should, in particular, not be retained; in other words, the adjacency effect should be included simultaneously. Of course, the application mode is only suitable for the decomposition of mixed pixels in single-band image data because the simulated scene only includes two types of objects, and studies of the PSF nonuniformity effect need to be further expanded to multi-band remote sensing images and multiple types of objects. In addition, the surface scene was simulated with a fixed radiation value for an object type, but some spectral variation is present in the actual image patches of object

types, which will interfere with the impact of the PSF nonuniformity and weaken the application of the uncertainty model.

6. Conclusions

Spectral unmixing has become one of the primary approaches for extracting the spatial distributions of surface parameters and is usually implemented based on the assumption of a uniform response of a sensor to surface radiation. However, the nonuniformity of a sensor's PSF is a basic feature of all remote sensors, and the study of the PSF nonuniformity effect is significantly important. Simulated data of the surface radiation distribution and a TM response matrix were developed to imitate the generation of mixed pixels and the extraction of the object proportion; the main conclusions are as follows:

(1) Under the nonuniformity effect of a sensor's PSF, the mixed-pixel DNs of a remote sensing image are random variables for the surface scene with identical object proportions and different distribution patterns, which is the primary cause of the nonuniformity effect of the sensor's PSF. When the true object proportion is 50%, the frequency distribution of the mixed-pixel DN is similar to a normal distribution function, whereas when the true proportion approaches 0% or 100%, its frequency distribution becomes asymmetrical, and the range of variation in the mixed-pixel DNs gradually diminishes.

(2) Under the nonuniformity effect of the sensor's PSF, models for the upper and lower bounds of the true proportion *versus* the estimated proportion at any probability level were established, which provided a probabilistic description of the uncertainty in spectral unmixing. The bound curves took the form of an asymmetrical spindle shape, and their degree of asymmetry gradually became larger as the confidence level increased.

(3) Under the nonuniformity effect of the sensor's PSF, the systematic error of the spectral unmixing refers to the difference between the estimated proportion and the average of the true proportion variations. There was a negative linear relationship between the systematic error of the spectral unmixing and the estimated value of the object proportion. At an estimated proportion of 50%, the systematic error of the proportion estimation was zero, and when the estimated proportion approached 0% or 100%, the object proportion was overestimated by 0.78% and underestimated by −0.78%, respectively.

(4) Under the nonuniformity effect of the sensor's PSF, the random error of the spectral unmixing was defined as the standard deviation of the true proportion in relation to the estimated proportion. There was a symmetrical polynomial functional relationship between the standard deviation of the spectral unmixing and the estimated value of the object proportion, opening downward. At an estimated proportion of 50%, the random error of the proportion estimation approached a maximum value of 4.4%, and as the estimated proportion approached 0% or 100%, the random error became a minimum of 1.05%.

The above study on the PSF nonuniformity effect was conducted based on a sensor's PSF with a unique fixed parameter of variance. Because there are some differences in the variances of different sensor PSFs, which take on different values in the track and scan directions, a future study should focus on the influence of the various parameters of the sensor's PSF on the nonuniformity effect in the extraction of object proportions. The impact of a sensor's PSF on spectral unmixing includes not only the nonuniformity effect, but also the adjacency effect, and the latter may have a greater influence; research on that topic will be discussed in detail in the companion article, "Simulation of the impact of a sensor's PSF on mixed pixel decomposition: 2. adjacency effect."

Acknowledgments: This study was funded by the Natural Science Foundation of China (Project No. 40671137) and the National High Technology Research and Development Program of China (Project No. 2009AA12Z136). We are grateful to the anonymous referees for their comments and suggestions on the first draft of the paper.

Author Contributions: Zhaoli Liu conceived of and designed the study. Chao Xu carried out the experiments. Chao Xu and Zhaoli Liu wrote the manuscript, and Guanglei Hou assisted with constructive discussions.

Conflicts of Interest: The authors declare no conflict of interest.

References

1. Strahler, A.H.; Woodcock, C.E.; Smith, J.A. On the nature of models in remote sensing. *Remote Sens. Environ.* **1986**, *20*, 121–139. [CrossRef]
2. Fisher, P. The pixel: A snare and a delusion. *Int. J. Remote Sens.* **1997**, *18*, 679–685. [CrossRef]
3. Cracknell, A. Review article Synergy in remote sensing-what's in a pixel? *Int. J. Remote Sens.* **1998**, *19*, 2025–2047. [CrossRef]
4. Quintano, C.; Fernández-Manso, A.; Shimabukuro, Y.E.; Pereira, G. Spectral unmixing. *Int. J. Remote Sens.* **2012**, *33*, 5307–5340. [CrossRef]
5. Duran, O.; Petrou, M. *Mixed Pixel Classification in Remote Sensing—Literature Survey*; School of Electronics and Physical Sciences, University of Surrey: Guildford, UK, 2004.
6. Manslow, J.F.; Nixon, M.S. *On the Ambiguity Induced by a Remote Sensor's PSF*; Wiley: Chichester, UK, 2002.
7. McGillem, C.; Anuta, P.; Malaret, E.; Yu, K. *Estimation of a Remote Sensing System Point-Spread Function from Measured Imagery*; LARS Technical Reports: West Lafayette, IN, USA, 1983; p. 81.
8. Markham, B.L. The Landsat sensors' spatial responses. *IEEE Trans. Geosci. Remote Sens.* **1985**, *6*, 864–875. [CrossRef]
9. Townshend, J.; Huang, C.; Kalluri, S.; Defries, R.; Liang, S.; Yang, K. Beware of per-pixel characterization of land cover. *Int. J. Remote Sens.* **2000**, *21*, 839–843. [CrossRef]
10. Schläpfer, D.; Nieke, J.; Itten, K.I. Spatial PSF Nonuniformity Effects in Airborne Pushbroom Imaging Spectrometry Data. *IEEE Trans. Geosci. Remote Sens.* **2007**, *45*, 458–468. [CrossRef]
11. Wu, H.-H.P.; Schowengerdt, R.A. Improved estimation of fraction images using partial image restoration. *IEEE Trans. Geosci. Remote Sens.* **1993**, *31*, 771–778. [CrossRef]
12. Huang, C.; Townshend, J.R.; Liang, S.; Kalluri, S.N.; DeFries, R.S. Impact of sensor's point spread function on land cover characterization: Assessment and deconvolution. *Remote Sens. Environ.* **2002**, *80*, 203–212. [CrossRef]
13. Kaiser, G.; Schneider, W. Estimation of sensor point spread function by spatial subpixel analysis. *Int. J. Remote Sens.* **2008**, *29*, 2137–2155. [CrossRef]
14. Turner, M.G.; Gardner, R.H.; O'neill, R.V. *Landscape Ecology in Theory and Practice*; Springer: New York, NY, USA, 2001.
15. Calle, A.; Casanova, J.-L.; Gonzalez-Alonso, F. Impact of point spread function of MSG-SEVIRI on active fire detection. *Int. J. Remote Sens.* **2009**, *30*, 4567–4579. [CrossRef]
16. Rauchmiller, R.F., Jr.; Schowengerdt, R.A. Measurement of the Landsat Thematic Mapper modulation transfer function using an array of point sources. *Opt. Eng.* **1988**, *27*, 334–343. [CrossRef]
17. Cliff, A.D.; Ord, J.K. *Spatial Processes: Models and Applications*; Pion Press: London, UK, 1981.
18. Pont, W.F.; Schwartz, C.R.; Crist, E.P.; Kenton, A.C. Sensor point spread function effects on the statistics of multispectral target signatures. In Proceedings of the SPIE's 1995 Symposium on OE/Aerospace Sensing and Dual Use Photonics, International Society for Optics and Photonics, Orlando, FL, USA, 17–21 April 1995; pp. 948–963.
19. Park, S.K.; Schowengerdt, R.A. Image sampling, reconstruction, and the effect of sample-scene phasing. *Appl. Opt.* **1982**, *21*, 3142–3151. [CrossRef] [PubMed]
20. Foody, G.M.; Doan, H.T.X. Variability in soft classification prediction and its implications for sub-pixel scale change detection and super resolution mapping. *Photogramm. Eng. Remote Sens.* **2007**, *8*, 923–933. [CrossRef]
21. Somers, B.A.; Asner, G.P.; Tits, L.; Coppin, P. Endmember variability in spectral mixture analysis: A review. *Remote Sens. Environ.* **2011**, *115*, 1603–1616. [CrossRef]